

Highlights from STAR (II)

- Hard Probes of the Initial and Final State -

Jörn Putschke for the STAR Collaboration¹

Yale University, Physics Department, New Haven, CT, USA, 06520-8120

Abstract

Highlights of recent results from the STAR collaboration focusing on hard probes of the initial and final state are presented. New results at forward rapidities in d+Au collisions at low x are utilized to study the possible onset of saturation effects at RHIC energies. New reference measurements, Υ production, nuclear- k_T via di-jets in d+Au collisions, and jet quantities in p+p collisions will be discussed. Final state nuclear modifications of J/ψ and identified hadrons in heavy-ion collisions will be presented. In addition to di(multi)-hadron and direct γ -hadron correlations, new results from full-jet reconstruction in Au+Au collisions will be discussed with respect to the p+p reference measurements. These measurements can be used to put further constraints on the underlying mechanisms of partonic energy loss in heavy-ion collisions at RHIC.

1. Introduction

Hard probes - processes involving large momentum transfers - and their modification in Au+Au collisions with respect to p+p (d+Au) can be used to study the properties of the medium created in a heavy-ion collision at RHIC energies [1]. In order to use hard processes as a well calibrated probe, one must be able to theoretically describe the reference measurements including initial and cold nuclear matter final state effects. The effect of parton energy loss in the final state is a well established observation in heavy-ion collisions at RHIC. It is evident in the suppression of the inclusive charged hadron and non-photonic electron yield at high- p_t , as well as in the associated yield in di-hadron correlations at high p_t^{trig} and p_t^{assoc} , accompanied by an enhancement at low p_t^{assoc} , suggesting a dramatic softening of jet fragmentation [2, 3, 4]. However, these measurements are limited in their sensitivity due to well-known geometric biases (see for example [5]). To overcome these biases one has to better constrain the parton kinematics, which is conceptually possible via direct γ - and full-jet reconstruction. New results utilizing these methods will be discussed.

In the following, new measurements addressing the initial state effects, such as the possible onset of saturation at low x , as well as improved reference measurements will be presented first. These will be followed by a discussion of how these calibrated hard probes become modified in the presence of the dense matter created in heavy-ion collisions at RHIC.

¹For the full list of STAR authors and acknowledgements, see appendix in this volume.

Email address: joern.putschke@yale.edu (Jörn Putschke for the STAR Collaboration)

19 2. Hard Probes of the initial state and p+p reference measurements

20 2.1. Forward rapidity measurements in p+p and d+Au collisions

21 Forward rapidity measurements in d+Au collisions can be used to study the possible onset of
 22 saturation effects at RHIC energies. The Forward Meson Spectrometer (FMS), new in 2008 (p+p,
 23 d+Au), is an electromagnetic calorimeter that probes processes down to $x \approx 10^{-4}$ at $\sqrt{s_{NN}}=200$
 GeV at around $\eta \sim 4$ [6], well into the range where saturation effects are expected to set in.

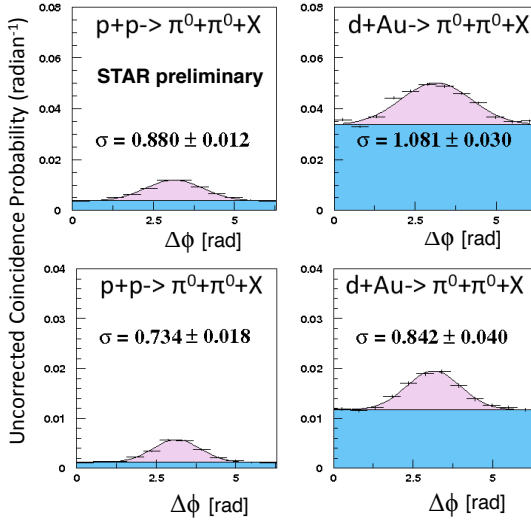


Figure 1: (color online) Uncorrected coincidence probability versus azimuthal angle difference between a forward π^0 (measured in the FMS) and a mid-rapidity π^0 (measured in the EMC) in p+p and d+Au collisions at $\sqrt{s_{NN}}=200$ GeV. Upper row: $p_t^{FMS} < 2 \text{ GeV/c}$ and $1 \text{ GeV/c} < p_t^{EMC} < p_t^{FMS}$; lower row: $p_t^{FMS} < 2.5 \text{ GeV/c}$ and $1.5 \text{ GeV/c} < p_t^{EMC} < p_t^{FMS}$.

24 By measuring the azimuthal angular correlations, $\Delta\phi$, of a forward π^0 and a mid-rapidity π^0
 25 one expects a clear back-to-back peak in a 2→2 parton scattering picture, whereas if saturation
 26 effects play a significant role a broadening of the recoil peak, or even its disappearance (monojet),
 27 could occur [7]. These effects can be measured by comparing the $\Delta\phi$ correlations from p+p with
 28 d+Au collisions as shown in Fig. 1. Two kinematic selections are shown in Fig. 1, one with a
 29 more restrictive cut (bottom panel), suggested by pQCD calculations [8], the other with a lower
 30 p_t cut closer to the saturation scale (top panel). The width of the recoil azimuthal correlation
 31 peak is larger for d+Au than for p+p and the difference ($\sigma_{dAu} - \sigma_{pp}$) increases from 0.11 ± 0.04
 32 to 0.20 ± 0.03 for the lower p_t cut, qualitatively consistent with a p_t dependent picture of gluon
 33 saturation in the Au nucleus (more details in [6]). In addition, the first observation of high- x_F
 34 J/ψ 's in p+p collisions at $\sqrt{s_{NN}}=200$ GeV have been reported by STAR at the conference [9].
 35

36 2.2. Υ measurement in d+Au collisions

37 The production of Υ and their modifications in heavy-ion collisions is a promising tool to
 38 study QGP properties at RHIC [10]. In addition to measurements in p+p and Au+Au it is im-
 39 portant to study possible cold nuclear effects on Υ production in d+Au collisions. The STAR
 40 Υ trigger enabled sampling a p+p equivalent luminosity of $\sim 12.5 \text{ pb}^{-1}$ for the 2008 d+Au run
 41 at $\sqrt{s_{NN}}=200$ GeV [11]. The measured signal of $\Upsilon(1S + 2S + 3S) \rightarrow e^+e^-$ shown in Fig.
 42 2 has a significance of $\sim 8\sigma$. The derived cross section at mid-rapidity is $B.R. \times d\sigma/dy =$
 43 $35 \pm 4(\text{stat.}) \pm 5(\text{sys.}) \text{ nb}$, consistent with NLO calculations [12]. The nuclear modification factor
 44 $R_{dAu} = 0.98 \pm 0.32(\text{stat.}) \pm 0.28(\text{sys.})$ suggests that Υ production follows binary scaling in d+Au

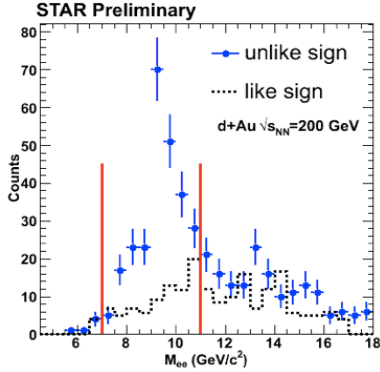


Figure 2: (color online) $\Upsilon \rightarrow e^+e^-$ signal and background in $\sqrt{s_{NN}}=200$ GeV d+Au collisions. The solid symbols with statistical error bars are obtained by combining the unlike-sign e^+e^- pairs. The dashed histogram shows the like-sign background.

45 collisions. With increased statistical significance these measurements will serve as an important
 46 reference for the upcoming measurement in Au+Au collisions (for more details see [11]).

47 2.3. Full-jet reconstruction in p+p and d+Au collisions

48 The study of jet properties and the underlying event in p+p collisions is important for our
 49 understanding of QCD and the not well understood process of hadronization, as well as providing
 50 a baseline for jet measurements in heavy-ion collisions.

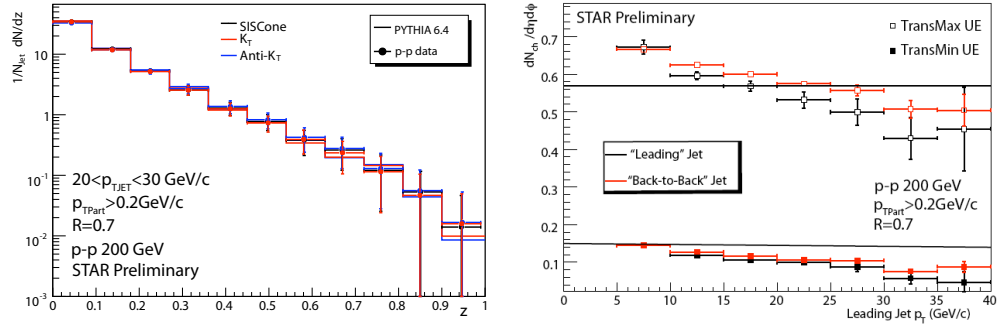


Figure 3: (color online) Left panel: Charged particle, detector level, $z = p_t^{hadron}/p_t^{jet}$ FF for jets reconstructed with $20 < p_{t,rec}^{jet} < 30$ GeV/c compared to PYTHIA for 3 different jet algorithms with $|\eta| < 1-R$ and $R=0.7$; right panel: the uncorrected charged particle density in the TransMin and TransMax regions as a function of reconstructed leading jet p_t , using the SIScone algorithm, with $R=0.7$.

51 Full jet reconstruction in STAR is performed by using charged particles, measured in the
 52 TPC, and neutral particles in the EMC at mid-rapidity. Modern jetfinding algorithms such as k_t
 53 and Anti- k_t recombination, and a seedless cone algorithm, SIScone, from the FastJet package
 54 [13] were used to reconstruct jets and to estimate systematic effects [14, 15, 16]. The jet energy
 55 resolution in p+p collisions can be obtained by either using PYTHIA simulations (PYTHIA
 56 6.410 Tune A [17]) passed through STAR's simulation and reconstruction algorithms, or via the
 57 jet energy balance of back-to-back di-jets in p+p data. Both methods result in a comparable
 58 jet energy resolution of $\sim 20\%$ for reconstructed jet with $p_t > 10$ GeV/c [14]. The uncorrected
 59 charged particle fragmentation function (FF) as a function of $z = p_t^{hadron}/p_t^{jet}$ for different res-
 60 olution parameters, R , and jet energies show reasonable agreement with PYTHIA for all jet

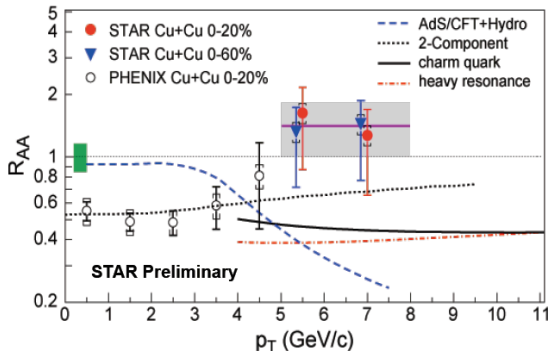


Figure 4: (color online) J/ψ R_{AA} vs. p_t in Cu+Cu collisions at $\sqrt{s_{NN}}=200$ GeV [22]. STAR data points have statistical (bars) and systematic (caps) uncertainties. The box about unity on the left shows R_{AA} normalization uncertainty, which is the quadrature sum of p+p normalization and binary collision scaling uncertainties. The solid line and band on the left plot show the average and uncertainty of the two 0-20% data points.

61 algorithms (see Fig. 3 left panel for $R = 0.7$). This agreement especially for larger R suggests
 62 that there are only minor NLO contributions beyond the PYTHIA LO calculations at RHIC en-
 63 ergies. We also studied the underlying event (UE) in p+p collisions following the CDF technique
 64 [18]. Fig. 3 (right panel) shows the charged particle density in the UE. One can conclude that
 65 the UE is largely independent of the jet energy. By comparing different selections and subsets in
 66 the UE analysis, which have different sensitivities to initial and final state radiation contribu-
 67 tions, we observe only minor contributions from large angle initial/final state radiation (further details
 68 in [14]).

69 Deploying full-jet reconstruction algorithms and methods to subtract background contribu-
 70 tions in the FastJet package we performed a measurement of nuclear k_t effects in d+Au colli-
 71 sions via di-jets [19]. To estimate the effect of jet energy resolution and possible background
 72 contributions of the underlying event in d+Au collisions on $k_{T,raw} = p_{T,1} \sin(\Delta\phi)$, we com-
 73 pared PYTHIA simulations and PYTHIA jets (including detector simulation) embedded in d+Au
 74 minimum bias events. This study suggests that jet energy resolution and possible background
 75 contributions in d+Au have only minor effects on the measured quantity [19]. We estimate a
 76 $\sigma_{k_{T,raw}} = 3.0 \pm 0.1(stat) \pm 0.4(sys)$ GeV/c in d+Au collisions at $\sqrt{s_{NN}}=200$ GeV. Further di-
 77 jet studies for different centralities in d+Au and p+p collisions will be pursued to estimate the
 78 nuclear k_t effects.

79 3. Hard Probes of the final state

80 3.1. Nuclear modification of J/ψ at high- p_t in Cu+Cu collisions

81 Suppression of J/ψ meson production in heavy-ion collisions has been proposed as a signa-
 82 ture of QGP formation [10]. The measured suppression at $\sqrt{s_{NN}}=200$ GeV [20] comparable to
 83 the observed magnitude at CERN-SPS energies is surprising and may be due to counterbalancing
 84 of larger dissociation with recombination of c and \bar{c} in the medium, which are more abundant
 85 at higher energies (see [12] and references within). To interpret the J/ψ suppression, an under-
 86 standing of quarkonium production in hadronic collisions is required. No model at present can
 87 fully explain the J/ψ production in elementary collisions. J/ψ measurements at high- p_t in p+p
 88 and Au+Au collisions may provide further insight into the underlying process of quarkonium
 89 production [9, 21]. In Fig. 4 the nuclear modification factor R_{AA} for J/ψ as function of p_t in
 90 Cu+Cu collisions at $\sqrt{s_{NN}}=200$ GeV is shown. The R_{AA} increases as a function of p_t and is
 91 consistent with unity for $p_t > 5$ GeV/c. The J/ψ is the only hadron measured in heavy-ion colli-
 92 sions at RHIC which does not exhibit a significant suppression at high p_t . The absence of J/ψ

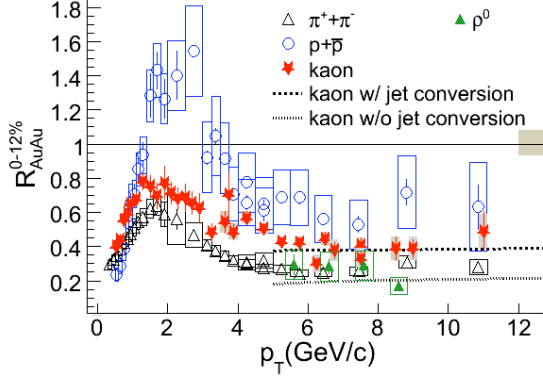


Figure 5: (color online) Nuclear modification factors R_{AA} of π , K , p and ρ in Au+Au collisions as a function of p_T . The bars and boxes represent statistical and systematic uncertainties.

93 suppression at high p_T , in contrast to a significant suppression of open charm, might indicate that
 94 high p_T J/ψ production is dominated by the color singlet channel (for more details on confronting
 95 theoretical calculations with the data see [21]). From high p_T J/ψ -hadron azimuthal correlations
 96 in p+p collisions one can estimate the contribution from B-meson feed-down to inclusive J/ψ
 97 production to be $13\% \pm 5\%$ for $p_T > 5$ GeV/c.

98 3.2. Jet flavor conversion in Au+Au collisions

99 To study the color charge effect of parton energy loss in heavy-ion collisions one can utilize
 100 the nuclear modification of identified hadrons (π , K and p) at high p_T . Figure 5 shows the nuclear
 101 modification factor R_{AA} in central Au+Au collisions at $\sqrt{s_{NN}}=200$ GeV as a function of p_T for π ,
 102 K and p [23]. One observes that the $R_{AA}(K)$ and $R_{AA}(p)$ are larger than $R_{AA}(\pi)$ in contradiction
 103 to predictions from energy loss calculations [24]. The observed ordering of R_{AA} for identified
 104 hadrons is consistent with predictions from calculations including jet flavor conversion in the hot
 105 dense medium [25] (see dashed lines in Fig. 5). In addition the identified hadron high- p_T spectra
 106 in p+p collisions are in agreement with NLO calculations and can be used to put constraints on
 107 the fragmentation functions (detailed discussion in [23]).

108 3.3. Di- and Multi-hadron correlations

109 The observation of the near-side ridge (long range $\Delta\eta$ correlation) has motivated many the-
 110 oretical attempts to explain this phenomena (for a summary see [26]). A recent model, the
 111 Correlated Emission Model (CEM) [27], suggested that the ridge is formed from correlated par-
 112 ticle emission due to aligned jet propagation and medium flow. As a consequence it predicts
 113 an asymmetric ridge $\Delta\phi$ correlation depending on the orientation with respect to the reaction
 114 plane $\phi_S = \phi_{trig} - \Psi_{RP}$. The measured ridge asymmetry (for details see [26]) as shown in Fig.
 115 6 (left panel) is qualitatively consistent with the CEM predictions suggesting that the ridge for-
 116 mation might be caused by jet-flow alignment. Updates concerning 3-particle near-side $\Delta\eta$ - $\Delta\eta$
 117 correlations, using the charge properties of the associated hadrons to separate the ridge and jet
 118 components, can be found in [26]. To study if the ridge is also present on the away-side, a tech-
 119 nique was developed where one uses a pair of correlated high- p_T hadron triggers to determine the
 120 jet-axis and study the associated hadron distribution (A) with respect to both triggers (T1 and T2)
 121 (details concerning the method can be found in [28]). Selecting a ‘‘symmetric’’ di-jet triggered
 122 case, $5 < p_T(T1) < 10$ GeV/c and $p_T(T2) > 4$ GeV/c, with $p_T(A) > 1.5$ GeV/c one observes no

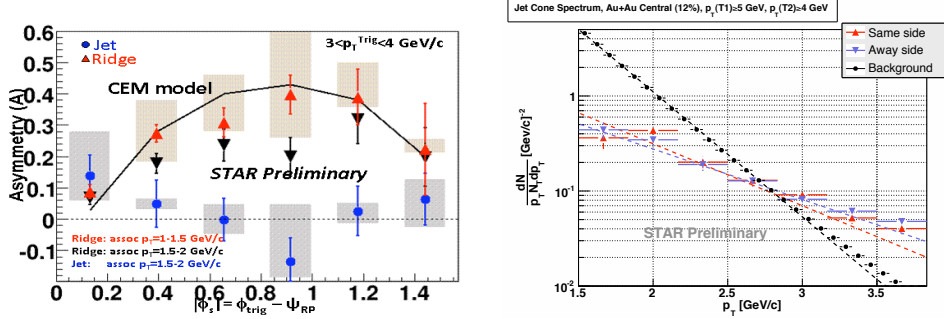


Figure 6: (color online) left panel: Asymmetry parameter for jet and ridge as a function of ϕ_s for 20-60% Au+Au collisions. The shaded bands represent the systematic uncertainties in the flow estimation. Also shown in black curve is the qualitative prediction from CEM (see text); right panel: Associated p_t spectra for the symmetric di-jet triggered correlations: $5 < p_t(T1) < 10$ GeV/c and $p_t(T2) > 4$ GeV/c with $p_t(A) > 1.5$ GeV/c. The red triangles represent the near-side and the blue inverted triangles the away-side correlation. Minimum bias background in black solid circles.

123 modification of the $\Delta\eta$ and $\Delta\phi$ correlations with respect to d+Au reference measurements, indi-
 124 cating that for this kinematical selection there is no evidence of a ridge or a conical structure on
 125 the away-side. For the symmetric di-jet selection the associated p_t spectra for both trigger sides
 126 are consistent (Fig. 6 right panel) and in agreement with d+Au measurements suggesting no, or
 127 only little, energy loss in the medium (more details in [28]).

128 3.4. Constraining the parton kinematics

129 The measurements discussed above are limited in their sensitivity to jet quenching effects
 130 due to well-known geometric biases. To gain sensitivity and to be able to distinguish between
 131 different underlying energy loss mechanisms, one has to better constrain the parton kinematics.
 132 This can be achieved via direct γ - and full-jet reconstruction measurements.

133 3.4.1. Direct γ -hadron fragmentation functions

134 Conceptually clean measurements to constrain the parton kinematics are direct γ -hadron (jet)
 135 correlations. Studies are however, limited in statistics, due to the small cross-section of that pro-
 136 cess. Details concerning the analysis can be found in [29]. In Fig. 7 the ratio of the integrated
 137 yield of associated charged hadron (h^\pm) per trigger in Au+Au relative to d+Au on the away-side
 138 ($D_{0-10\%}/D_{d+Au}$) for π^0 and direct γ ($8 < p_t^{\gamma,\pi^0} < 16$ GeV/c) as function of $z_T = p_T^{assoc}/p_T^{trig}$
 139 at $\sqrt{s_{NN}}=200$ GeV is shown. In the measured z_T kinematics there is no apparent difference in the
 140 suppression of π^0 - h^\pm and direct γ - h^\pm correlations. Naively one would expect a difference due to
 141 the trigger bias of the high- p_t π^0 's, which would result in a longer pathlength of the recoil jet
 142 in the π^0 - h^\pm case. The absence of this effect might be due to a significant contribution of punch
 143 through or tangential jets in the measured kinematical regime, which would leave the fragmenta-
 144 tion function unmodified. The measurements are in agreement with theoretical calculations (see
 145 [29] and references within), but to distinguish between the different models one has to extend the
 146 measurement to lower z_T , which we plan to pursue.

147 3.4.2. Full-jet reconstruction in Au+Au collisions

148 Full-jet reconstruction in heavy-ion collisions is an alternative approach to constrain the par-
 149 ton kinematics over a larger range of jet energies as compared to direct γ -hadron (jet) correla-
 150 tions. The challenges in these measurements are to correct for contributions from the underlying

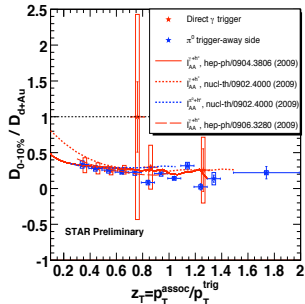


Figure 7: (color online) Ratio $D_{0-10\%}/D_{d+Au}$ of π^0 and direct γ ($8 < p_T^{\gamma,\pi^0} < 16$ GeV/c) as function of z_T at $\sqrt{s_{NN}}=200$ GeV compared to the theoretical calculations (see text).

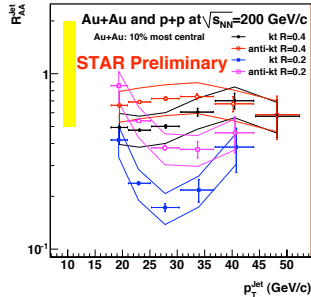


Figure 8: (color online) R_{AA} of jets reconstructed with k_t and anti- k_t algorithms for the two different resolution parameters.

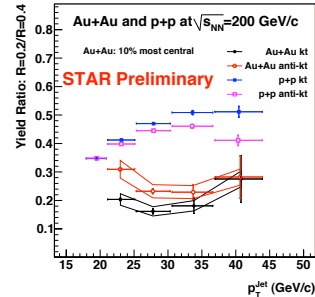


Figure 9: (color online) Jet cross-section in p+p and Au+Au reconstructed with $R = 0.2$ divided by cross-sections reconstructed with $R = 0.4$ for k_t and anti- k_t algorithms .

151 heavy-ion event. In central Au+Au events at $\sqrt{s_{NN}}=200$ GeV the background energy in a cone
 152 of 0.4 is ~ 45 GeV/c and fluctuations in the background are of the order of $\sigma = 6 - 7$ GeV/c
 153 [15, 16]. A data driven correction scheme for background contributions and detector effects
 154 was developed, including a first attempt to estimate the corresponding systematic uncertainties
 155 [14, 15, 16]. In the case of unbiased jet reconstruction in heavy-ion collisions, one would expect
 156 a scaling of the inclusive jet cross-section with the number of binary collisions N_{bin} . The results
 157 shown in in Fig. 8 and Fig. 9 changed as compared to what was shown at the Quark Matter Confer-
 158 ence, for further discussion see [15]. In Fig. 8 the R_{AA} of jets reconstructed with the k_t and
 159 anti- k_t algorithm [13] for resolution parameters $R = 0.2$ and 0.4 is shown as a function of jet p_T .
 160 It is notable that with full-jet reconstruction the kinematic reach to study jet quenching effects
 161 is greatly extended, up to jet p_T 's of ~ 45 GeV/c in central Au+Au collisions. For $R = 0.4$ one
 162 recovers a larger fraction of jets as compared to the inclusive hadron R_{AA} and to $R = 0.2$. This
 163 measurement indicates that an unbiased jet population is not recovered for $R = 0.4$ in central
 164 Au+Au collisions, even though the systematic uncertainties are still quite large. An alternative
 165 explanation to an overall absorption, could be a significant jet broadening beyond $R = 0.4$, which
 166 would lead to an underestimation of the reconstructed jet energy in Au+Au with respect to p+p
 167 at $\sqrt{s_{NN}}=200$ GeV. Fig. 9 shows, by comparing the cross-section ratios in p+p and Au+Au of
 168 jets found with $R = 0.2$ normalized to $R = 0.4$, that there is a broadening in the jet structure.
 169 Assuming a continues evolution, this suggests that there might be a significant contribution for
 170 $R > 0.4$. This assumption is in agreement with the observed significant suppression in the di-jet
 171 coincidence measurements (see Fig. 10, left panel), where the path-length and therefore the effect
 172 of parton energy loss of the recoil jet is maximized by utilizing the trigger bias of the online
 173 triggered events (see [16]). The absence of strong modifications in the fragmentation function
 174 measurements (see Fig.10, right panel) can also be explained by a significant broadening in the
 175 jet structure due to energy loss.

176 4. Summary

177 In these proceedings a wealth of new measurements from the STAR collaboration were pre-
 178 sented utilizing hard probes to study the initial and final state effects. The possible onset of

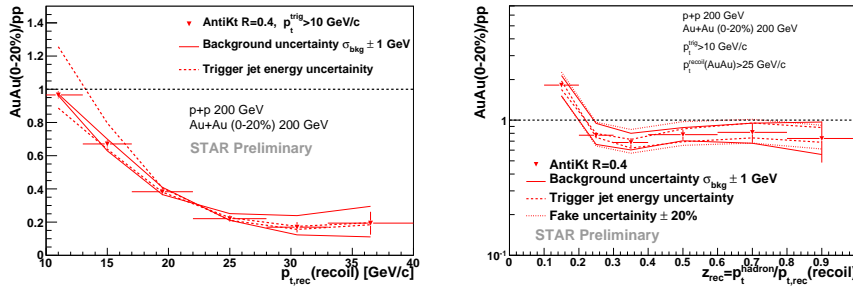


Figure 10: (color online) Left panel: Ratio of di-jet coincidence in Au+Au over p+p reference measurements ; right panel: Fragmentation function ratio Au+Au over p+p as a function of z for $p_t^{recoil} > 25$ GeV/c.

179 saturation effects, as well as new and improved baseline measurements of the initial state, were
 180 discussed. The presented data of nuclear modifications in the final state can be used to gain
 181 further insights into the production mechanisms of heavy-flavor. Full-jet reconstruction extends
 182 significantly the kinematical reach to study jet quenching effects and modifications of jet quan-
 183 tities in the presence of the hot, dense medium created in heavy-ion collisions at RHIC. These
 184 measurements will put further constraints on the underlying partonic energy loss mechanisms.

185 References

- 186 [1] J. Adams et al. (STAR), Nucl. Phys. **A757**, 102 (2005), nucl-ex/0501009
 187 [2] J. Adams et al. (STAR), Phys. Rev. Lett. **97**, 162301 (2006), nucl-ex/0604018
 188 [3] J. Adams et al. (STAR), Phys. Rev. Lett. **95**, 152301 (2005), nucl-ex/0501016
 189 [4] B.I. Abelev et al. (STAR), Phys. Rev. Lett. **98**, 192301 (2007), nucl-ex/0607012
 190 [5] T. Renk, K. Eskola, Phys. Rev. **C75**, 054910 (2007), hep-ph/0610059
 191 [6] E. Braidot (STAR) (2009), These proceedings.
 192 [7] D. Kharzeev, E. Levin, L. McLerran, Nucl. Phys. **A748**, 627 (2005), hep-ph/0403271
 193 [8] V. Guzey, M. Strikman, W. Vogelsang, Phys. Lett. **B603**, 173 (2004), hep-ph/0407201
 194 [9] C. Perkins (STAR) (2009), These proceedings.
 195 [10] T. Matsui, H. Satz, Phys. Lett. **B178**, 416 (1986)
 196 [11] H. Liu (STAR) (2009), These proceedings.
 197 [12] A.D. Frawley, T. Ullrich, R. Vogt, Phys. Rept. **462**, 125 (2008), 0806.1013
 198 [13] M. Cacciari, G.P. Salam, G. Soyez, JHEP **04**, 005 (2008), hep-ph/0802.1188
 199 [14] H. Caines (STAR) (2009), These proceedings.
 200 [15] M. Ploskon (STAR) (2009), These proceedings.
 201 [16] E. Bruna (STAR) (2009), These proceedings.
 202 [17] T. Sjostrand, S. Mrenna, P. Skands, JHEP **05**, 026 (2006), hep-ph/0603175
 203 [18] A. Cruz (CDF) (2005), PhD Thesis, University of Florida.
 204 [19] J. Kapitan (STAR) (2009), These proceedings.
 205 [20] A. Adare et al. (PHENIX), Phys. Rev. Lett. **98**, 232301 (2007), nucl-ex/0611020
 206 [21] D. Kikola (STAR) (2009), These proceedings.
 207 [22] B.I. Abelev et al. (STAR) (2009), 0904.0439
 208 [23] Y. Xu (STAR) (2009), These proceedings.
 209 [24] X.N. Wang, Phys. Rev. **C58**, 2321 (1998), hep-ph/9804357
 210 [25] W. Liu, C.M. Ko, B.W. Zhang, Phys. Rev. **C75**, 051901 (2007), nucl-th/0607047
 211 [26] P. Netrakanti (STAR) (2009), These proceedings.
 212 [27] C.B. Chiu, R.C. Hwa, Phys. Rev. **C79**, 034901 (2009), 0809.3018
 213 [28] K. Kauder (STAR) (2009), These proceedings.
 214 [29] H. Ahmed (STAR) (2009), These proceedings.